



Deep learning rapid flood risk predictions for climate resilience planning



Ahmed Yosri ^{a,b,c}, Maysara Ghaith ^{a,b,c,*}, Wael El-Dakhakhni ^{a,b,d}

^a Department of Civil Engineering, McMaster University, 1280 Main Street West, Hamilton, ON L8S 4L7, Canada

^b Interdependent Network Visualization, Simulation, Optimization and Machine Learning Laboratory (INViSiONLab), 1280 Main Street West, Hamilton, ON L8S 4L7, Canada

^c Department of Irrigation and Hydraulics Engineering, Faculty of Engineering, Cairo University, Giza 12613, Egypt

^d School of Computational Science and Engineering, McMaster University, 1280 Main Street West, Hamilton, ON L8S4K1, Canada

ARTICLE INFO

Keywords:

Climate Resilience
Deep learning
Flood Risk
Hierarchical Neural Network
Vulnerability Assessment

ABSTRACT

Floods have been causing the world's costliest weather-related catastrophes and their magnitude and frequency are projected to increase even further due to climate change. Current flood risk quantification procedures include the use of complex and highly uncertain hydrologic-hydraulic models for hazard mapping and computationally-tedious manipulations for vulnerability evaluation—hindering urban centers climate resilience planning. Adopting a novel approach that bypasses such time-consuming procedures, this study presents a deep learning-based rapid and accurate flood risk prediction tool, RAPFLO, to directly relate flood risk characteristics (level, extent, and likelihood) to their main drivers (e.g., climate, topography, and land cover). The approach employed to develop RAPFLO is generic in nature and the associated methodology is not site-dependent. To demonstrate its utility, RAPFLO is deployed on the City of Calgary, Canada, and is used to reproduce the fluvial flood risk across the city between the years 2010 and 2020. RAPFLO efficiently replicated the risk level with an overall accuracy of 80 % and the risk likelihood with a coefficient of determination of 0.96. Subsequently, RAPFLO was employed for predicting future fluvial flood risk from the year 2025 to 2100 under the RCP 8.5 climate scenario. RAPFLO presents a valuable computationally efficient, accurate, and rapid decision support system that empowers city managers and infrastructure operators to devise effective climate resilience strategies considering different climate projections and future *what-if* scenarios.

1. Introduction

Global warming and population growth over the last two centuries have led to a drastic change in the earth's climate that subsequently results in intensifying the consequences and increasing the frequency of weather extremes (Anaraki et al., 2021; Hosseinzadehtalaei et al., 2021; Zandalinas et al., 2021). Over the past five years, the World Economic Forum has been ranking such extremes among the top global risks in terms of likelihood, impacts, and long-term threat to humans (McLennan, 2021; 2022). Such an alarming situation led most nations to allocate specific funds for climate change adaptation (Buchanan et al., 2022), penalize excessive greenhouse gas emissions (Cheng et al., 2021), and shift strategic priorities to the sustainable and resilient development (Fekete et al., 2021).

Floods are one of the most prevalent, costliest, and devastating weather-related extremes that can propagate over large areas (Gaur et al., 2018; b; Nofal and van de Lindt, 2020), resulting in a high number

of causalities, widespread economic losses, and severe and lasting health problems (Ekmekcioglu et al., 2022; Li et al., 2020). Once realized, a flood can cause major catastrophe based on the complex interplay between meteorological (e.g., precipitation), physical (e.g., elevation and slope), and anthropogenic (e.g., population, land use) attributes (Ekmekcioglu et al., 2022; Wan Mohtar et al., 2020). Flood risk is thus concerned with the probable consequences of two distinct systems interactions: the hazard and the exposed/vulnerable elements-at-risk (Dewan, 2013). This can be represented mathematically as the convolution of inundation probability (reflecting the hazard) and the probability of potential adverse consequences to the system (representing the losses associated with the exposed/vulnerable elements-at-risk) over the area of interest (Eini et al., 2020).

The first contributor of flood risk is the built system vulnerability resulting from the interaction between factors pertaining to population (e.g., size, demography, gender distribution), buildings (e.g., age, structure, material), critical infrastructure (e.g., roads, bridges, public

* Corresponding author at: Department of Civil Engineering, McMaster University, 1280 Main Street West, Hamilton, ON L8S 4L7, Canada.
E-mail address: ghaithm@mcmaster.ca (M. Ghaith).

service units), and topography (e.g., elevation, land use, land cover). Such factors are generally grouped under social, economic, and physical vulnerabilities (Aroca-Jiménez et al., 2022; Balica et al., 2009; Cho and Chang, 2017; Membele et al., 2022), and are typically weighted using subjective (i.e., knowledge-based) or objective (i.e., data-driven) methods. Subjective (e.g., analytical hierarchical process) and objective (e.g., entropy method, catastrophe theory, principal component analysis) weighting methods aim at identifying the relative importance of each vulnerability-contributing factor based on expert knowledge and internal statistical structure, respectively (Ziarh et al., 2021). Subjective methods may result in biased weights, and therefore their objective counterparts are most often preferred when the required data is available (Ziarh et al., 2021). A coupled objective-subjective weighting scheme can also be used, where a combined factor importance is evaluated through multiplying the weights from both approaches (Jenifer and Jha, 2017; Wu et al., 2022) or through a game theoretic-based interconnection (Lai et al., 2015). The total system vulnerability is subsequently calculated as the weighted summation of contributing factors after normalization based on a suitable scheme (e.g., z-score, minmax, ranking).

The second contributor of flood risk is the hazard magnitude that can be evaluated using physics-based or data-driven approaches (Chen et al., 2021; Ghaith et al., 2022a; Kabir et al., 2020; Norallahi and Seyed Kaboli, 2021; Verma et al., 2023; Yan et al., 2021; Zhou et al., 2021; Ziarh et al., 2021). Physics-based approaches rely on the hydrologic modeling of contributing watersheds (i.e., rainfall-runoff modeling) followed by a hydraulic simulation of the main river systems within the area (i.e., runoff-inundation simulation). The employed hydrologic and hydraulic models are typically calibrated using ground-truth observations, albeit separately without considering the interactions between the two models (Li et al., 2021). However, an integrated calibration process is necessary to reduce uncertainties associated with models' parameters, structures, and inputs (Li et al., 2021). Once calibrated, physics-based hydrologic-hydraulic models are employed to calculate hazard probabilities corresponding to specific depth thresholds under different flood scenarios. Despite the proven utility of physics-based flood hazard mapping approaches, existing development and calibration procedures of hydrologic and hydraulic models are complex, uncertain, time-consuming, and computationally intensive particularly for large study areas (Zhou et al., 2021).

In contrast to physics-based flood hazard mapping techniques, their data-driven counterparts aim at correlating the frequency of specific locations being flooded to their hydrologic (e.g., precipitation) and topographic (e.g., slope, elevation, distance to water body) characteristics using a statistical, mathematical, or supervised machine learning models. Examples of such models include random forest-based regression trees (Feng et al., 2015; Hou et al., 2021; Marco et al., 2022), support vector regression (Eini et al., 2020; Jang et al., 2022; Mehravar et al., 2023), multivariate statistical approaches (Youssef et al., 2016), and maximum entropy (Norallahi and Seyed Kaboli, 2021). Although the efficiency of such approaches has been confirmed for urban flood hazard mapping, their application to fluvial floods remains limited to date. Recently, with the development of more efficient deep learning and evolutionary computing techniques, fluvial inundation has been accurately related to river inflows using convolution neural networks (Chen et al., 2021; Ghaith et al., 2022a; Kabir et al., 2020; Liao et al., 2023; Yan et al., 2023), long-short-term memory networks (Rasheed et al., 2022; Zhang et al., 2023; Zhou et al., 2021; Zou et al., 2023), self-organizing maps (Chang et al., 2022; 2021; Jhong et al., 2022), and two-dimensional genetic programming (Yan et al., 2021).

Despite the efficacy of existing physics-based and data-driven flood hazard mapping techniques, their adaptability to fluvial flood risk prediction under climate change requires integration with climate models. Such integration, however, requires careful consideration of the different spatiotemporal scales of the underlying hydrologic, hydraulic, and climatic processes. In addition, further model recalibration/

retraining should be conducted based on inputs from employed climate models. These drawbacks of physics-based and data-driven flood hazard mapping approaches restrict their utility for fluvial flood risk prediction considering the climate change impacts (da Silva et al., 2020; Komolafe et al., 2018). As such, most of the related studies focused on simplifying the climate-hydrologic-hydraulic interactions to roughly evaluate the fluvial flood risk for certain flooding scenarios (e.g., for a range of return periods) using hydrologic/hydraulic modeling (e.g., Cea and Costabile, 2022; Oubennaceur et al., 2021; Pasquier et al., 2019) or through statistically relating the probability of flood risk to contributing variables such as rainfall, land use, and demographic changes (e.g., da Silva et al., 2022). However, in order to accurately estimate the fluvial flood risk under climate change, a continuous real-time simulation is required, which typically requires an extensive amount of data and processing time.

The objective of this study is to develop an accurate rapid flood risk prediction tool, RAPFLO, utilizing the hierachal deep neural network (HDNN). The underlying methodology of RAPFLO aims at directly estimating the fluvial flood risk level and likelihood based on implicitly simulating the complex interactions between the factors associated with the flood hazard and the built system vulnerability. RAPFLO's methodology is thus generic by nature and can be applied to any area given that data required for the development of the HDNN in RAPFLO is available. To demonstrate its utility, RAPFLO was employed to reproduce the annual fluvial flood risk level and likelihood due to propagating waves in the Bow and Elbow Rivers in the City of Calgary, Canada, between the years 2010 and 2020. Trained, validated, and tested, RAPFLO was subsequently used to predict probable future floods and their characteristics along with their associated monetary losses between the years 2025 and 2100 under the RCP 8.5 climate change scenario. Assuming slow urban development and demographic changes within the considered area, RAPFLO can be used for the long-term prediction of fluvial flood risks. However, information about planned or projected developments and expected future demographic variability across the selected area can be included prior to RAPFLO development or be continuously fed to RAPFLO as inputs in order to accommodate the corresponding impacts. Once tuned/trained, RAPFLO empowers urban center decisionmakers to proactively devise effective climate resilience planning strategies, infrastructure managers to prepare sustainable management plans, and city residents to plan proper long-term investments to mitigate the risk of fluvial floods.

2. Methods

As described earlier, risk is quantified based on the hazard magnitude alongside the exposed system response. Under a flood event, the hazard magnitude is related to the physical properties of contributing catchments, land use, as well as the expected amount of rainfall. On the other hand, the system response under floods is determined based on the inherent physical and socioeconomic vulnerabilities, as shown in Fig. 1. Although a flood event can impact two neighboring locations/attributes (e.g., buildings), the resulting adverse consequences (i.e., resulting flood risk) can significantly differ based on the corresponding vulnerability. This section thus describes the typical procedure of predicting the flood risk likelihood as well as the underlying methodology of developing RAPFLO, and is divided into four subsections. The first subsection discusses how the flood vulnerability is generally quantified within an area of interest regardless of the characteristics of the flood event. The second subsection illustrates the typical approaches of estimating and mapping the flood hazard probability. The third subsection describes the integration of flood vulnerability and hazard probability for flood risk quantification. Finally, the fourth subsection explains how RAPFLO integrates the different contributing elements to directly quantify the flood risk characteristics (i.e., level, likelihood) using deep learning. It should be highlighted that while the fourth subsection (i.e., RAPFLO development) represents the primary contribution of the present study,

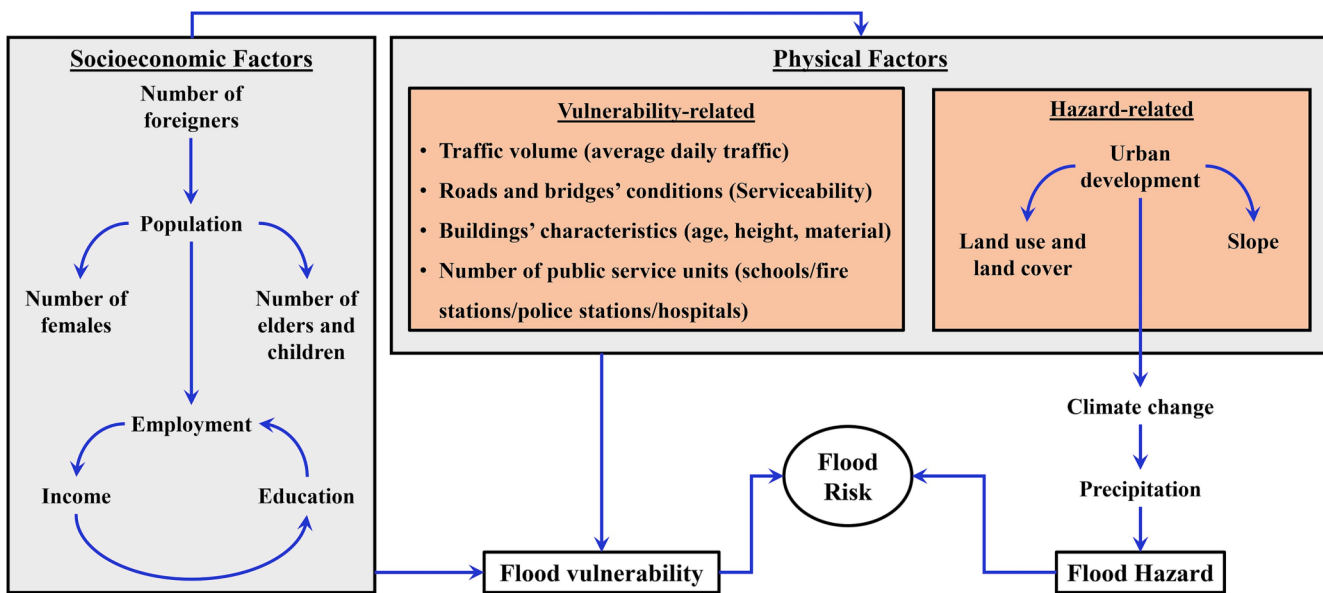


Fig. 1. Factors affecting the flood risk and interactions between them.

the other three subsections have also been detailed for completeness.

2.1. Vulnerability assessment

Personal and public assets and critical infrastructure that are both exposed and vulnerable (damageable due) to a certain hazard realization usually fall under one of three vulnerability categories: social, economic, and physical. Such categories can be dealt with separately or collectively. Vulnerability typically changes from one location to another depending on several contributing factors (e.g., population size, socioeconomic status, infrastructure conditions). The importance and understanding of such factors vary based on data availability, spatial diversity, and/or government legislation pertaining to data collection. Social vulnerability reflects the level of population inability to combat and cope with the impacts of a certain hazard realization (Lianxiao and Morimoto, 2019), whereas social resilience reflects their ability to rapidly recover from subsequent disaster. Both the social vulnerability and social resilience levels depend on the intrinsic characteristics of population (e.g., age, gender, health conditions, employment, and education). Economic vulnerability measures the community capacity to withstand the economic consequences of hazard realizations (e.g., loss of jobs, inflation) (Aroca-Jiménez et al., 2018; Fuchs et al., 2019). Finally, physical vulnerability refers to the expected level of buildings and critical infrastructure performance under specific hazard impacts and is generally quantified based on type, activity, location, age, and asset value of the infrastructure (Aroca-Jiménez et al., 2022; Papathoma-Köhle et al., 2022).

In order to quantify the total vulnerability of an urban center (or attributes within an urban center) to natural hazard, all relevant factors need to be normalized and subsequently aggregated into an overall vulnerability index (VI). Normalization techniques (e.g., ranking, z-score, minmax, categorization) aim at standardizing categorical and numerical data such that the inherited bias is omitted (Emdad Haque et al., 2022; Moreira et al., 2021). Ranking normalization technique is used to map categorical variables into latent numerical ones. Normalization based on z-score rescales the mean and standard deviation of a numerical variable into zero and one, respectively. Minmax is another normalization technique for rescaling numerical variables between zero and one. Categorization is used for both numerical and categorical variables and relies on dividing the data into subsets using certain percentiles.

Following normalization, vulnerability-contributing factors are

weighted based on subjective or objective approaches. Subjective weighting approaches rely on experts' opinions and are typically applied following statistical surveys. Alternatively, factors may be weighted equally when limited information is available. Such weighting approaches can thus result in biased importance weights and subsequently misleading conclusions. To avoid this drawback, objective weighting approaches convert the factors' internal statistical structures into unbiased weights. Examples of such approaches include the principal component analysis (PCA) and entropy method (EM). Despite only employing the latter, and since either of these objective approaches is typically applied for vulnerability quantification with no privilege for one over the other, detailed descriptions of both are provided herein for completeness.

The PCA is typically performed through investigating the covariance structure of the normalized factors. Eigenvectors and corresponding eigenvalues are subsequently calculated based on the variance-covariance matrix, and principal components (PCs) are then estimated through multiplying the eigenvectors (weight of factors in PCs) and the original normalized factors. The weight of each normalized factor is subsequently determined based on the number of PCs required to achieve a prespecified threshold of variance explained (i.e., summation of normalized eigenvalues after being ranked in a descending order) (Yu et al., 2021a). When multiple PCs are required, eigenvectors are weighted based on the corresponding fraction of variance explained and the vulnerability factors are weighted accordingly (Yu et al., 2021b). Location-based VI values are subsequently estimated as the weighted summation of corresponding vulnerability factors.

The EM presents another objective approach to evaluate the weights of vulnerability factors, and depends on measuring the valuable information provided by each factor (Zhang et al., 2014; Zhu et al., 2020). Entropy is used to measure the inherent uncertainty in random variables (Pal and Pal, 1991; Purvis et al., 2019), and was employed in a wide range of applications such as thermodynamics (Misra et al., 1979; Yelon et al., 2006), biological experiments (Boomsma et al., 2014), urban systems (Purvis et al., 2019), and water network and water quality systems (Keum et al., 2018; 2017; Ursulak and Coulibaly, 2021). The entropy value ranges between zero and one, with higher values reflecting more inherent variability, more informative explanations, and thus higher factor weight. To apply the EM for vulnerability evaluation, the dataset corresponding to each contributing factor needs to be allocated to different bins based on a predetermined classification method (e.g., Jenks natural break, quantile, standard deviation, equal interval). The

entropy value and corresponding weight are subsequently calculated using Equations (1) and (2), respectively (Zhu et al., 2020):

$$E_i = -\frac{\sum_{j=1}^n X_{ij} \ln(X_{ij})}{\ln(n)} \quad (1)$$

$$w_i = \frac{1 - E_i}{\sum_{i=1}^m (1 - E_i)} \quad (2)$$

where X_{ij} is the representative value of the factor i in bin j , E_i is the entropy of factor i , w_i is the weight of factor i , n is the number of bins, and m is the number of factors. Similar to vulnerability evaluation based on the PCA, entropy-based weights calculated using Equation (2) are multiplied by corresponding factor values and the total VI is subsequently evaluated as the summation of weighted factors. It should be highlighted that VI values are evaluated across the study area at the spatial scale where contributing factors are collected. It should be also emphasized that when the VI is evaluated at a fine scale (e.g., at the building scale), it can be upscaled to a grid, neighborhood, or community level using arithmetic, geometric, weighted mean, or other upscaling schemes.

2.2. Flood hazard modeling

Hazard modeling is an essential step to determine the level and likelihood of subsequent climate-induced risks. For fluvial floods, flood hazard maps can be produced based on the hydraulic modeling of main river systems considering the routing mechanism and overland flow. Physics-based hydraulic models employ upstream flow gauges, city and river topology obtained from digital elevation models (DEM), and land use/cover to mimic the underlying physical processes and subsequently produce inundation depth maps. Alternatively, flood inundation can be directly related to observed inflow at upstream locations in a data-driven fashion, as proposed in recent studies (e.g., Kabir et al., 2020; Kumar et al., 2023; Liao et al., 2023; Yan et al., 2023; 2021; Zhang et al., 2023). As the time lag between flood realization and observed river inflow is typically short (i.e., in the range of hours), linking flood characteristics to the inception of the causing precipitation is key to

enable meaningful (rapid) preparedness and subsequently ensure community resilience. However, prior to initiating the hydraulic modeling, one needs to conduct hydrological modeling, employing meteorological data (e.g., precipitation, temperature), watershed properties (i.e., topography, slope, and streams), and land use/cover to develop a rainfall-runoff relationship. The main output from a hydrologic model is the stream flow at a single or multiple locations—representing the main input for the subsequent hydraulic modeling. Fig. 2 summarizes the typical procedures applied for flood hazard prediction based on hydrologic-hydraulic modeling.

It should be highlighted that calibrating both the hydrologic and hydraulic models is necessary to enable the replication of ground-truth stream flows and inundation depths. Although the calibration process is typically conducted for each model separately, such an approach neglects a fundamental aspect—that hydrologic and hydraulic processes are naturally coupled. Integrated (coupled) calibration is thus key but is nonetheless challenging because of the different spatiotemporal scales at which the contributing factors are collected as well as its exorbitant computational cost.

2.3. Risk quantification

Risk integrates the uncertain natures of hazard, exposure, and vulnerability with induced losses defined through a stage-damage curve. A stage-damage curve represents a monotonically increasing relationship between flood depth and the expected cost of resulting damages (Scawthorn et al., 2006; Smith, 1994). It should be emphasized that a stage-damage curve is an intrinsic characteristic of the underlying system/component (e.g., building, power substation, transportation infrastructure) and thus do not change according to the system proximity to the hazard source. As the flood risk is evaluated through the convolution of inundation probability and expected consequences (represented by the VI), the stage-damage curve is discretized into specific regions with increasing risk levels. For each risk level (flood depth and damage ranges), the corresponding likelihood is evaluated through multiplying the inundation probability and component specific VI value. It should be emphasized that the resulting risk level and likelihood maps have the same spatial resolution of the employed inundation depth and VI values.

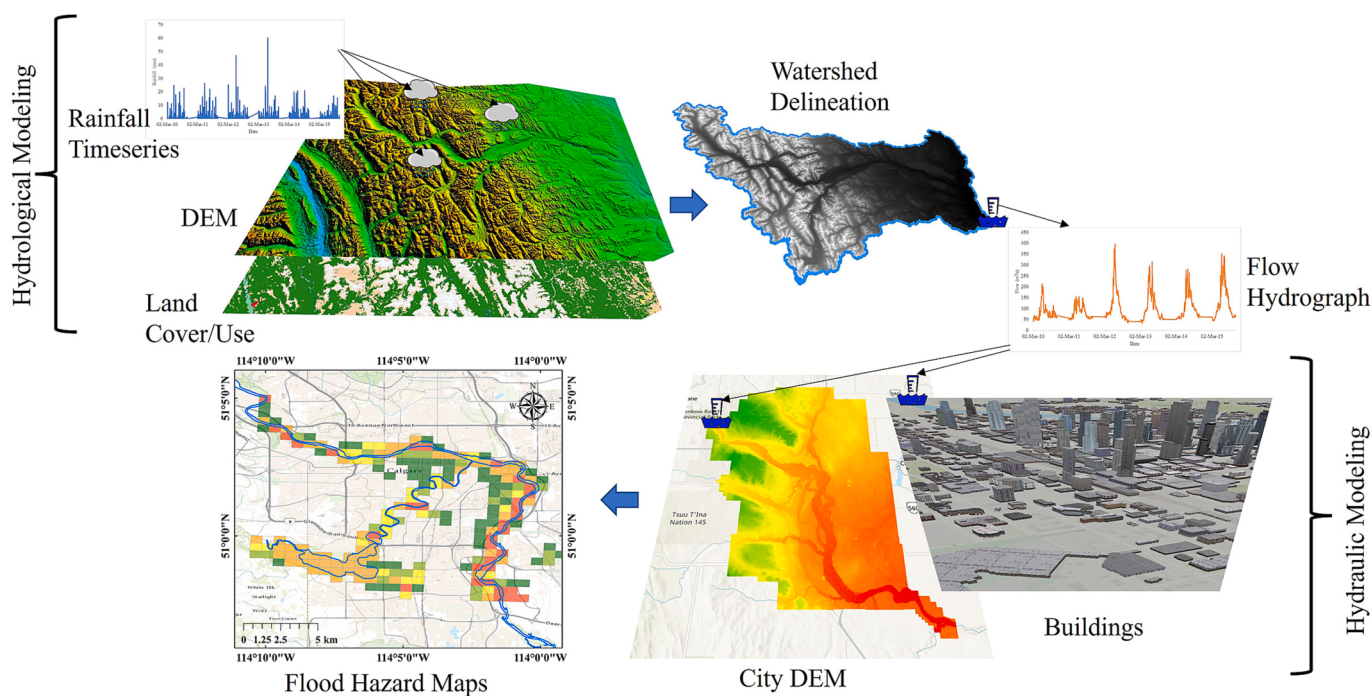


Fig. 2. Physics-based flood hazard mapping methodology.

It should be also highlighted that when different components (e.g., residential buildings and public health units) exist within the same spatial scale (i.e., the grid cell), a representative stage-damage curve should be identified based on the component importance, vulnerability, asset value, or based on an extensive fragility assessment considering all components.

2.4. RAPFLO architecture

As described earlier, flood risk estimation requires multiple sequential steps that include VI evaluation, rainfall-runoff modeling (i.e., hydrologic modeling), runoff-inundation simulation (i.e., hydraulic modeling), and finally flood hazard probability evaluation. RAPFLO is developed employing a hierarchical deep learning approach (i.e., HDNN) to bypass such computationally expensive steps, with application to fluvial flood risk prediction considering climate change.

2.4.1. Inputs and outputs

The main challenge pertaining to the development of any data-driven flood risk prediction model is to identify the inputs controlling the corresponding output as well as adjusting the model parameters and architecture such that actual outputs are efficiently reproduced. For fluvial flood risk prediction, the model outputs should be the risk characteristics (i.e., level and likelihood). On the other hand, inputs to the model should reflect the magnitude and spatiotemporal aspects of the hazard as well as the spatial variability of the VI. As the main goal of RAPFLO is to provide climate-driven risk predictions, the

spatiotemporal drivers of flood hazard have been represented through precipitation-focused climate indices (e.g., statistics of the precipitation amount, the number of wet days) at various locations. The spatial variability of the VI is reflected through the ground elevation, slope, land use/cover, and distance from the nearest river/water body.

2.4.2. RAPFLO computational core

RAPFLO relies on a HDNN to explore the complex non-linear relationships between a set of inputs and outputs. The HDNN is a feed-forward back-propagation artificial neural network, albeit it employs several hidden layers (hence the notion of deep neural network) with sizes increasing hierarchically alongside the input and output layers utilized in other neural network architectures (Fig. 3a). In addition, an activation function is adopted prior to the output layer to rescale the outputs from the hidden layers such that the actual observations are matched as accurate as possible (Haykin, 1999).

Similar to other data-driven and machine learning models, models employing such network architecture may suffer from overfitting. The phenomenon of overfitting occurs when the model predictability is limited to the data used for development, restricting its generalizability. As such, training, validation, and testing subsets are typically prepared, where the former two subsets are used during the model development stage whereas the latter subset is adopted to evaluate the model predictability of an independent, unseen (i.e., out-of-sample) dataset. During the model development stage, additional techniques can be incorporated to reduce the risk of overfitting such as early stopping and regularization (Zanotti et al., 2019), cross validation and feature

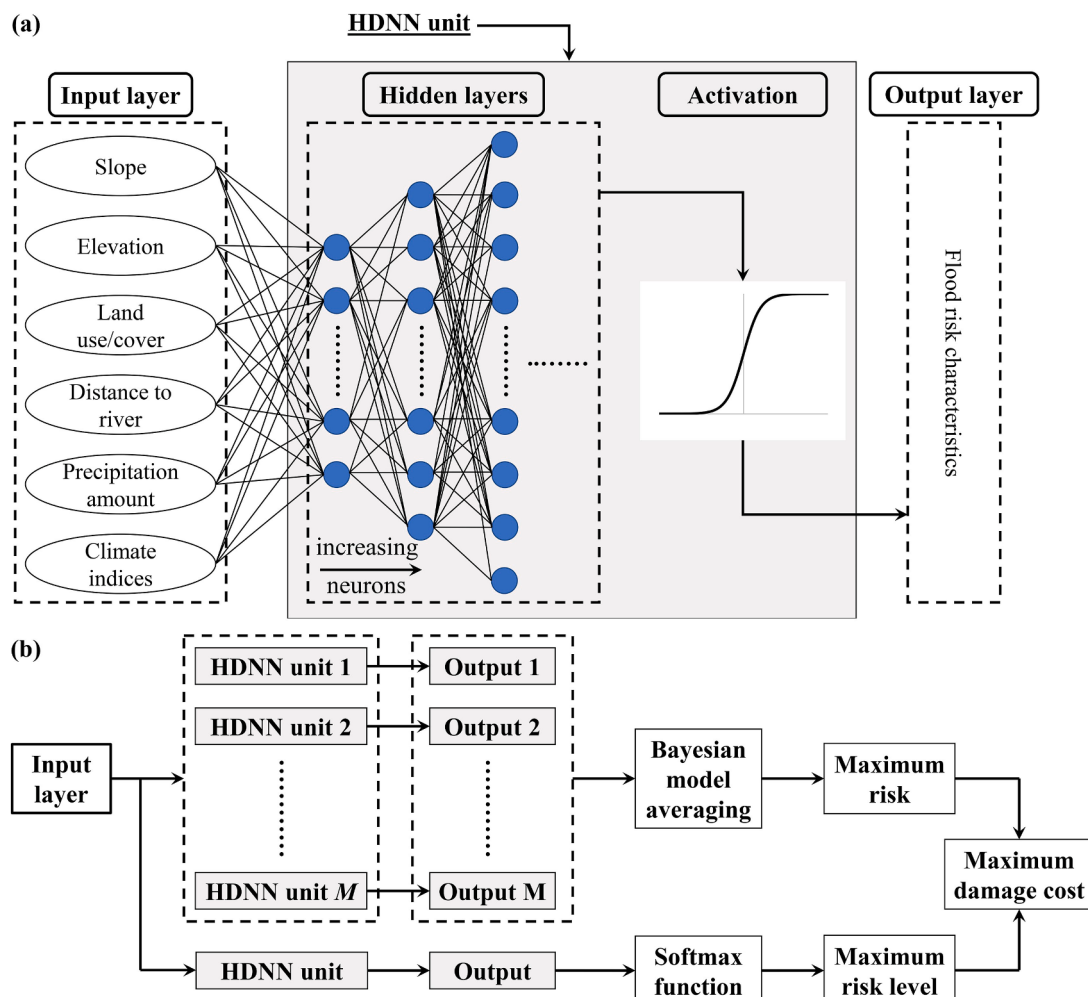


Fig. 3. (a) The typical architecture of the HDNN and (b) a schematic of RAPFLO developed in this study.

selection (He et al., 2023), as well as the use of dropout layers (Srivastava et al., 2014).

Since the fluvial flood risk is characterized in this study through flood level and likelihood, two different HDNN-based models are developed (Fig. 3b). The first is regression-based and is used to estimate the risk likelihood (probability), whereas the second model is a classification-based HDNN to predict the risk level (severity). The coefficient of determination (R^2) is adopted to evaluate the performance of the first model, whereas the precision, recall, and f-score are employed to assess the predictability of the second one.

2.4.3. Ensemble predictions

It should be noted that HDNN-based models typically require a long training time that can be significantly reduced attributed to the ongoing advances in computational capabilities (e.g., parallel processing, graphics processing units). However, network (i.e., model) parameters are still optimized locally as the global convergence requires extensive amount of observed input-output pairs, which is challenging due to the typically limited data collection and documentation/digitization resources. A HDNN-based model is thus parameterized several times, based on different initializations, and corresponding outputs are subsequently combined. This implies the development of M number of HDNNs, and subsequently blinding the resulting outputs based on a predetermined scheme. Several ensemble approaches can be used for such purpose, with the Bayesian model averaging (BMA) technique has shown superiority in several applications (Duan et al., 2007; Raftery et al., 2005). It should be highlighted that the number of models employed (i.e., M) within the BMA technique is typically selected such that significant improvements in the blinded output is no longer

observed when the value of M increases. The statistics (e.g., mean, standard deviation) of the blinded output(s) are thus monitored as the value of M increases, and the optimal value is selected once such quantities stabilize. It should be highlighted that the BMA is only applied to combine the outputs from regression-based HDNNs (i.e., used for flood risk likelihood estimation) and is not adopted alongside classification-based HDNNs due to the categorical nature of the latter's output. It should be also noted that the architecture of RAPFLO (Fig. 3) makes it generic by nature, and generalizable in the sense that it can be deployed to any city given that input and output data required for training the embedded HDNN-based models are available. In addition, once trained/tuned for a specific site (i.e., implicitly accounting for the specific site parameters including hydrologic, hydraulic, topographic, asset value distribution, etc.), the tuned model is also generalizable in the sense it can be used to predict future flood event losses, function of future unseen climate conditions, that might occur in that site/city. As such, RAPFLO, while generic in its approach, and is generalizable to predict future events for specific sites, it requires training/tuning for different sites/cities considering the vast differences, in terms of the hydrologic, hydraulic, topographic, and asset value distribution from one city to another.

3. Study area characteristics and data preparation

The City of Calgary, Canada was selected as a testbed in this study to demonstrate the efficiency of RAPFLO, where the data required to calculate the risk components (i.e., hazard and vulnerability) and associated damages (i.e., cost) are described in the following subsections. Calgary is the third-largest city and fifth-largest metropolitan

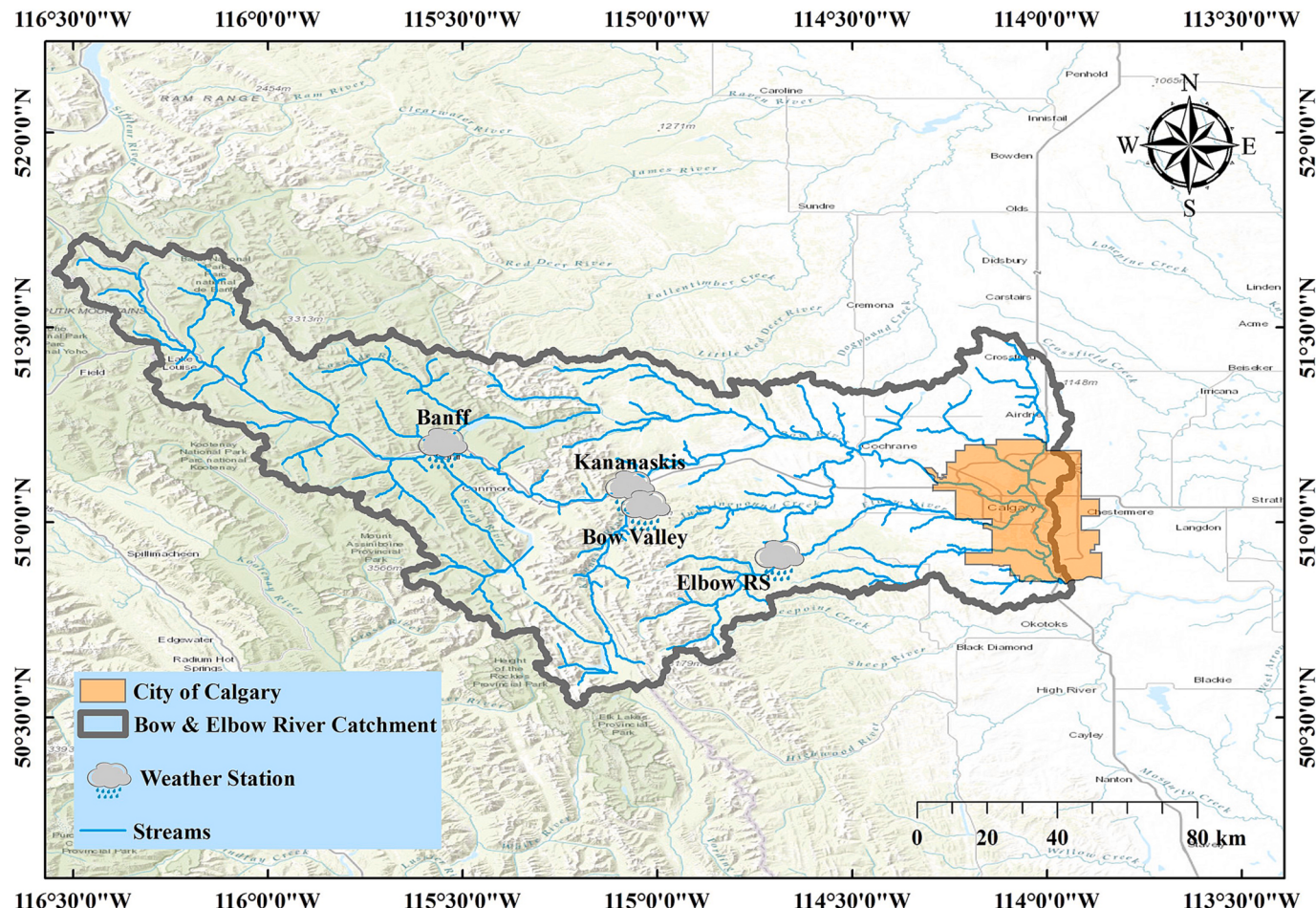


Fig. 4. Bow and Elbow River Catchments affecting the City of Calgary.

area in Canada with an urban population and a year-over-year population increase of around 1.4 million and 0.66 %, respectively (Calgary, 2021). The city is located at the confluence of the Bow and Elbow rivers characterized by average peak daily flows of $612 \text{ m}^3/\text{s}$ and $292 \text{ m}^3/\text{day}$ (based on records between 1911 and 2020), respectively, that occur seasonally between May and September (Government of Canada, 2022). The Bow and Elbow rivers have a collective catchment area upstream the city of Calgary of about $11,000 \text{ km}^2$, as shown in Fig. 4. Such a relatively large watershed area associated with its geographical location near the Canadian Rocky Mountains render parts of the City of Calgary high-flood-risk areas (Mohanty and Simonovic, 2021). For example, the City of Calgary has been impacted by devastating flood events in 2005 and 2013, with the latter resulted in more than \$5B economic losses and caused the evacuation of around 100,000 people (Gaur et al., 2018a; b). Improving existing flood forecasting techniques and developing new flood risk prediction tools have therefore been highlighted as key strategies for combating fluvial flood events (Khan et al., 2018). Such techniques and tools can support the sustainable development in urban centers and enhance their resilience under expected climate-induced fluvial floods.

3.1. Vulnerability evaluation

In this study, the fluvial flood vulnerability in the City of Calgary is evaluated based on ten social factors, two economic measures, and ten physical attributes, as shown in Table 1. All of these metrics are publicly available through the City of Calgary's open data portal (<https://data.calgary.ca/>), and are provided at different spatial scales (i.e., component, community, and ward levels). A grid of $500 \text{ m} \times 500 \text{ m}$ square cells is therefore assumed to overlay the City of Calgary and vulnerability contributing factors are assigned to each cell according to the following: 1) factors defined at the component level (i.e., building asset value, household income, road length, traffic volume, number of historic places, number of bridges, land use, building age, number of service units, land cover) are assigned directly to each of the overlaying cells; 2)

Table 1
Features used for vulnerability evaluation and corresponding entropy-based weights.

Feature classification	Feature definition	Weight
Social	Number of non-official language speakers	0.078
	Number of vulnerable people (younger than 19 and older than 55)	0.073
	Number of foreigners	0.065
	Number of females	0.064
	Number of unemployed persons	0.063
	Population size	0.063
	Number of people without post-secondary education	0.060
	Fraction of population with residential unit ownership	0.034
	Number of employed persons	0.021
	Number of people with post-secondary education	0.021
Economic	Building asset value	0.040
	Household income	0.028
Physical	Road length	0.051
	Traffic volume	0.050
	Number of historic places	0.047
	Number of bridges	0.043
	Urban density	0.038
	Land use	0.036
	Building age	0.034
	Number of service units	0.033
	Land cover (flow resistance)	0.032
	Expected damage severity based on the stage-damage curve	0.027

factors defined at the community (i.e., population size, demography, and non-official language speakers) and ward (i.e., employment, education, foreign nationality) levels are distributed across the overlaying cells based on the residential density.

Following standardization based on the *minmax* normalization approach, each factor is weighted using the *entropy method* as described earlier. The top six ranked (i.e., most important) factors are the number of non-official language speakers, vulnerable people, foreigners, females, unemployed persons, followed by the total population size. The remaining factors have comparable weights without a clear cut-off, indicating the importance of including all factors for vulnerability evaluation. The VI is thus evaluated at the center of each grid cell as the summation of contributing factor values after being multiplied by the corresponding entropy-based weights shown in Table 1, and a map of the resulting cell-based VI values is shown in Fig. 5. Most of the areas within the City of Calgary are less vulnerable to fluvial floods (around 74.7 % of the area has a VI value of less than 10%) and are scattered across the city. In contrast, Calgary's areas that are highly susceptible to fluvial floods are located at a very short distance around the Bow River, which coincides with the on-site flood conditions investigated following the 2013 devastating event. It should be emphasized that the scatter nature of VI values observed across the city of Calgary (Fig. 5) suggests the heterogeneity of the factors presented in Table 1, supporting the decision of including all of them for vulnerability evaluation.

3.2. Flood hazard data and probability estimation

As described before, hazard maps required for fluvial flood risk quantification can be produced through the application of either physics-based or data-driven hydraulic or hydrologic-hydraulic models. When hydraulic models are employed, model calculations are constrained using flow/head data. On the other hand, a hydrologic-hydraulic model is used to directly convert precipitation data into inundation depths. Recently, a two-dimensional physics-based hydraulic model was developed by Ghaith et al., (2022b) for inundation depth prediction in the City of Calgary. The model geometry, locations of boundary conditions, and calibration stations are shown in Fig. 6. This model was developed using the opensource software HEC-RAS® and was calibrated (Ghaith et al., 2022b) as follows: 1) the domain is divided into two regions with different Manning's coefficient values, and 2) the calibration parameter (i.e., Manning's coefficient) values were varied based on a trial-and-error procedure until inundation depth estimates at the calibration stations (i.e., stations 05BM015, 05BJ001, and 05BH004 shown in Fig. 6) and the maximum flood extent matched those observed during the 2013 flood event (Fig. 7a). It should be highlighted that as Manning's coefficient is uncertain by nature, efficient model calibration is crucial to minimize the impact of such uncertainty on the model estimates and performance (Huang and Liang, 2006). A multicriteria calibration process Ghaith et al., (2022b) was thus adopted where the hydraulic model was calibrated based on inundation depths observed at discrete locations within the study area together with the flood extent across the whole domain. It should be also highlighted that different sets of calibration parameters may result in similarly performing hydrologic/hydraulic models (i.e., the principle of equifinality), and thus related studies suggested aggregating the corresponding estimates into a single output based on a predetermined scheme (Ahmadi et al., 2019; Ficklin and Barnhart, 2014). Such a procedure has not been employed in this case study as its main focus is to demonstrate the utility of RAPFLO as a prediction tool. However, the principle of equifinality can be incorporated within RAPFLO through using aggregated model estimates during the training and validation of the HDNN used in RAPFLO. The hydraulic model developed and calibrated by Ghaith et al., (2022b) was accordingly utilized in this study to estimate daily inundation depths between 2010 and 2020 (sample inundation depth maps are shown in Fig. 7), where flow values at the upstream boundary condition locations (i.e., 05BH005, 05BJ004, and 05BK001) are obtained from the City of

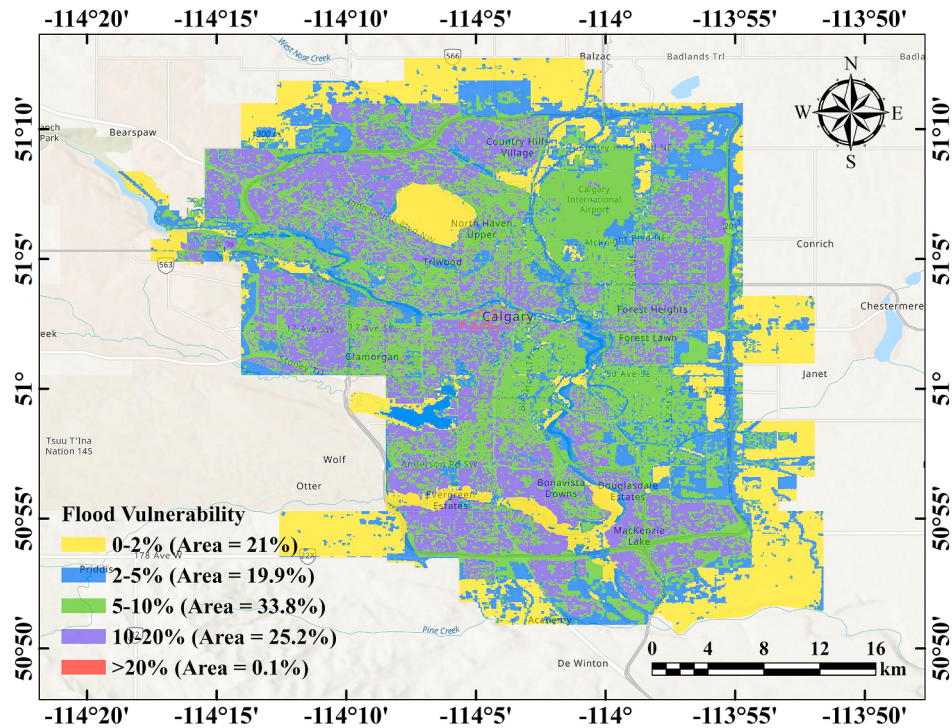


Fig. 5. Entropy-based fluvial flood vulnerability index (VI) across the city of Calgary.

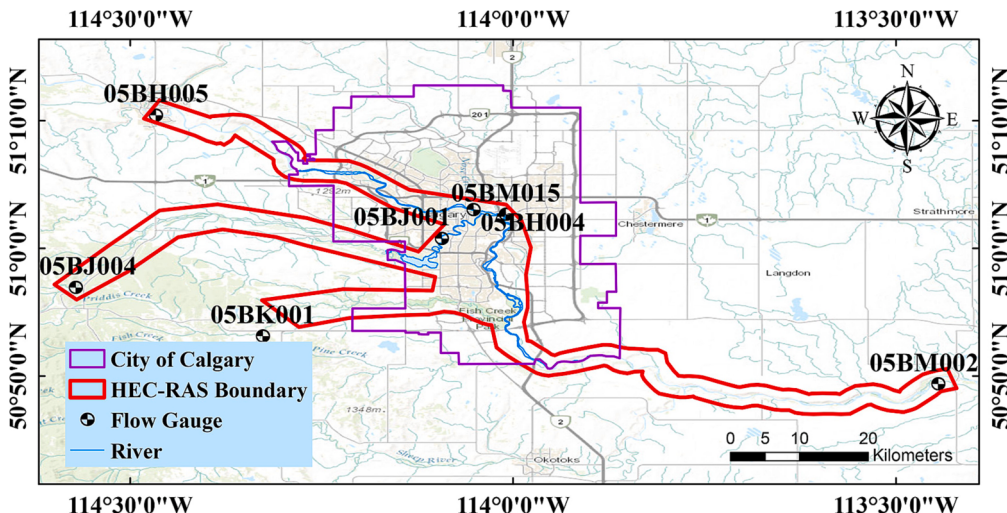


Fig. 6. HEC-RAS model geometry, boundary condition locations (i.e., 05BH005, 05BJ004, 05BK001, and 05BM002), and station used for calibration (i.e., 05BM015, 05BJ001, and 05BH004).

Calgary's Open Data Portal (<https://data.calgary.ca/>). It should be highlighted that the HEC-RAS model employed in this study required several hours to estimate the spatial distribution of daily inundation depths for one year only, which represents a single subprocess within the risk quantification procedure.

A property-specific stage-damage curve is typically used to relate the inundation depth to the corresponding cost of induced damage, as shown in Fig. 8. For the City of Calgary, stage-damage curves for residential and commercial buildings have been developed by Golder Associates in 2015 and are publicly available through the Government of Alberta's Open Data Portal (<https://open.alberta.ca/>). It should be highlighted that costs provided in such stage-damage curves are based on the money value in 2014. As the objective of this study is to predict the fluvial flood risk level, likelihood, and corresponding induced

damage, each stage-damage curve is discretized into five risk levels (i.e., very low, low, medium, high, and very high) based on the induced damage cost (Fig. 8). For each of these risk regions: i) the corresponding hazard probability is calculated as the frequency of daily inundation depths between associated lower and upper depth limits; and ii) the mean damage cost is used as a representative damage value and is defined based on the money value in 2014.

The hazard probability for each risk level and corresponding damage cost as well as the building type is assigned to each cell within the overlaying grid. As multiple building types may exist within the same grid cell, a dominant type is identified. Such dominant type is determined through the simultaneous ranking of all types in a descending order based on the associated asset value and ascendingly based on the inundation depth corresponding to the total loss condition (d_{max} in

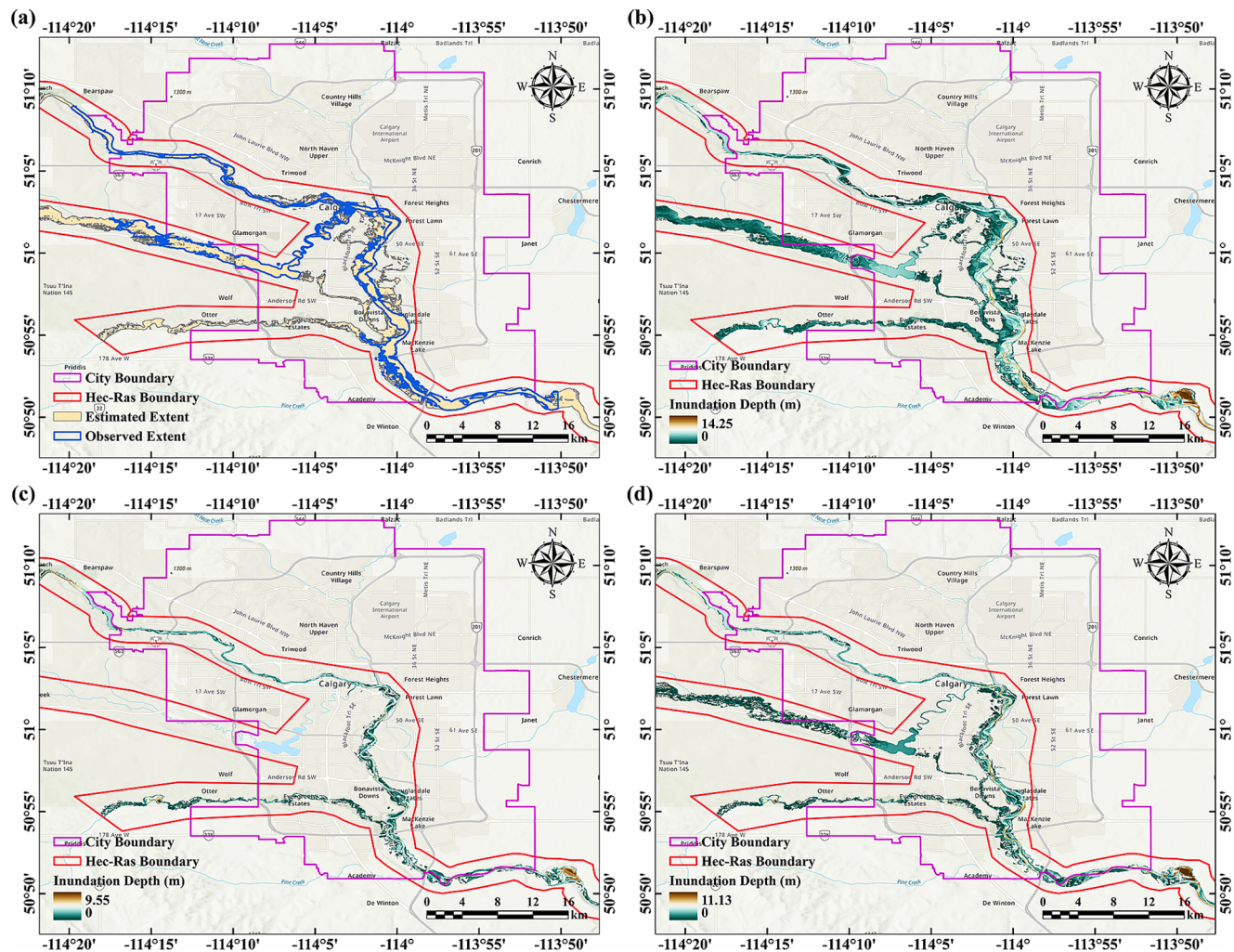


Fig. 7. HEC-RAS model estimates: (a) flood extent in 2013 and inundation depth in (b) 2013, (c) 2016, and (d) 2020.

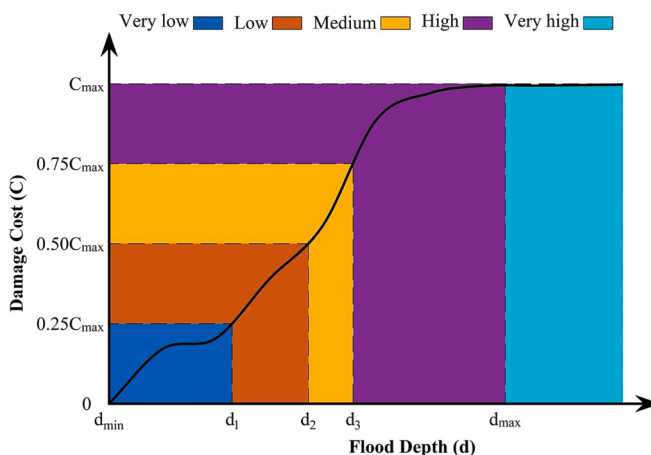


Fig. 8. Typical stage-damage curve used in this study.

Fig. 8). The dominant building type assigned to each cell is shown in Fig. 9.

3.3. RAPFLO inputs and outputs

As described before, the computational core of RAPFLO is a HDNN that consists of multiple hidden layers with sizes increasing sequentially

and is trained based on risk level and likelihood between 2010 and 2020. Inputs to the HDNN include physical attributes (i.e., elevation, slope, infiltration resistance, and distance to the nearest river) and annually-evaluated climate indices reflecting the main precipitation characteristics. Ground elevations are represented through a 2 m DEM provided publicly through the city of Calgary's open data portal (<https://data.calgary.ca/>). These elevations are assigned to each cell within the city boundary, where the arithmetic mean is used when multiple DEM points exist within the same cell. Average ground slope is calculated at the center of each cell based on the elevation difference and cell-to-cell distance considering all neighboring cells. Infiltration resistance is a measure of the land ability to enhance or inhibit the runoff following a rainfall event and is a function of the land cover. Infiltration resistance data are provided through the open portal of the City of Calgary (<https://data.calgary.ca/>).

Climate indices employed in this study include the annual number of days with precipitation larger than 1 mm and larger than 10 mm, the maximum daily precipitation in cool, warm, and overwintering seasons, and the maximum precipitation volume accumulated over ten days in cool, warm, and overwintering seasons. Such indices are obtained at the four weather stations shown in Fig. 4 (Banff, Bow Valley, Elbow RS, Kananaskis). In lieu of other climate indices developed over the past decade, the adopted indices have been suggested for evaluating climate impacts at the local and regional scales (Li et al., 2018). In addition, precipitation indices are employed in this study instead of a complete list of climate indices (i.e., precipitation and temperature) as the former are

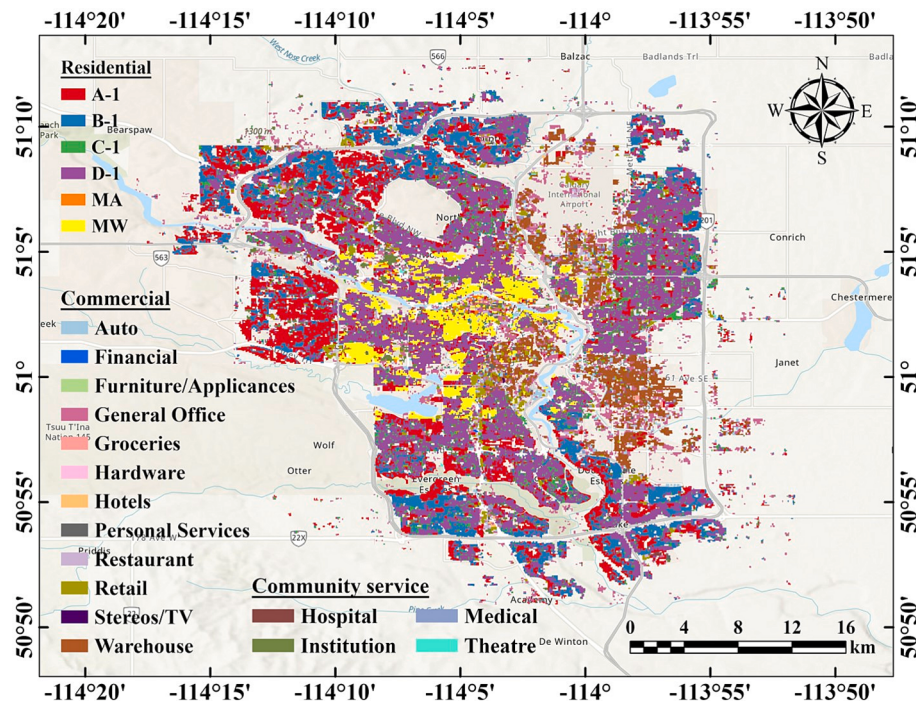


Fig. 9. Dominant building type in each cell.

more relevant to floods. Furthermore, precipitation indices are evaluated annually by definition, and thus such a time resolution has been adopted in the present study during both the model development and prediction stages. For the training, validation, and testing of the regression- and classification-based HDNNs (between 2010 and 2020), climate indices employed in this study are calculated based on daily precipitation and temperature records available through the open climate data portal of Canada (<https://climatedata.ca/>). On the other hand, for prediction purposes between 2025 and 2100, such indices are replaced by the 5th, 25th, 50th, 75th, and 95th percentiles of the corresponding ensemble calculated based on 24 global climate models. Indices from each of these models are obtained from the Government of Canada's open data portal (<https://canada.ca/>) and are already down-scaled statistically to 10 km × 10 km resolution using the bias correction analogues method.

As physical attributes inputted to the HDNN (i.e., mean elevation, average ground slope, infiltration resistance, and distance to the river) vary spatially not temporally whereas climate indices are station-related but change over time (i.e., vary spatiotemporally), every climate index considered was scaled by each of the physical factors employed through a pair-wise mathematical multiplication evaluated at the cell level. Such integration procedures have resulted in 128 input variables (8 climate indices × 4 weather stations × 4 physical attributes) at each grid cell, with a total number of 58,944 data points that are subsequently divided into training (70 % represented by 41,260 input–output pairs), validation (15 % represented by 8,842 input–output pairs), and testing (15 % represented by 8,842 input–output pairs) subsets. On the other hand, outputs from the HDNN include the maximum risk level and corresponding likelihood at each grid cell. For model development and testing purposes, such outputs are evaluated as follows: 1) the VI values shown in Fig. 5 are multiplied by the hazard probabilities for each risk level shown in Fig. 8, resulting in a corresponding risk likelihood; 2) the maximum likelihood is subsequently evaluated for each cell in every year from 2010 to 2020; and finally 3) the corresponding risk level is determined. Scaled climate indices, maximum risk level, and risk likelihood are then paired based on the cell location and year of interest, formulating the input–output pairs required for the training, validation, and testing of the regression- and classification-based HDNNs. It should

be highlighted that risk characteristics (likelihood and level) are not measurable metrics per se; instead, they are typically estimated through convolving the VI using the hazard probability as described above. Risk characteristics quantified in such a way thus represent the reference values and are therefore referred to as the actual metrics hereafter. On the other hand, risk characteristics predicted using the developed HDNN-based models are referred to as estimates and are subsequently compared to the actual ones to evaluate the model performance. It should be noted that each of the HDNNs employed encompasses four hidden layers with sizes equal 40, 50, 60, and 70, respectively, where the root mean squared error (RMSE) is adopted as the model performance criterion. Such sizes were selected through a trial-and-error procedure such that a high model performance (i.e., lower RMSE value and higher R^2 value) is achieved in a timely manner. Each HDNN is trained using the scaled conjugate gradient algorithm through which the network parameters (i.e., weights and biases of the neurons in the different hidden layers) are adjusted based on the conjugate descending gradient direction of the error function (Johansson et al., 1992).

4. Results and discussion

4.1. Historical flood risk prediction

Both the regression- and classification-based HDNNs within RAPFLO were trained, validated, and tested using, respectively, 70 %, 15 %, and 15 % of the data from the period between 2010 and 2020, where samples within each subset are allocated randomly. For risk likelihood estimation, 100 regression-based HDNNs are developed for the same training, validation, and testing subsets, albeit with different initial values for the network parameters. This number of HDNNs was arbitrarily selected in this study for demonstration purposes only; however, the proper number can be determined through monitoring the statistics of the model outputs as described earlier. The BMA technique is subsequently applied based on the training and validation subsets only, where the resulting weights ranged between 1×10^{-3} and 0.18 with a 5th and 95th percentile of 1.3×10^{-3} and 0.05, respectively. As shown in Fig. 10, the HDNN-BMA ensemble accurately reproduced the actual maximum risk likelihood with an R^2 value of 0.96 for all of the training,

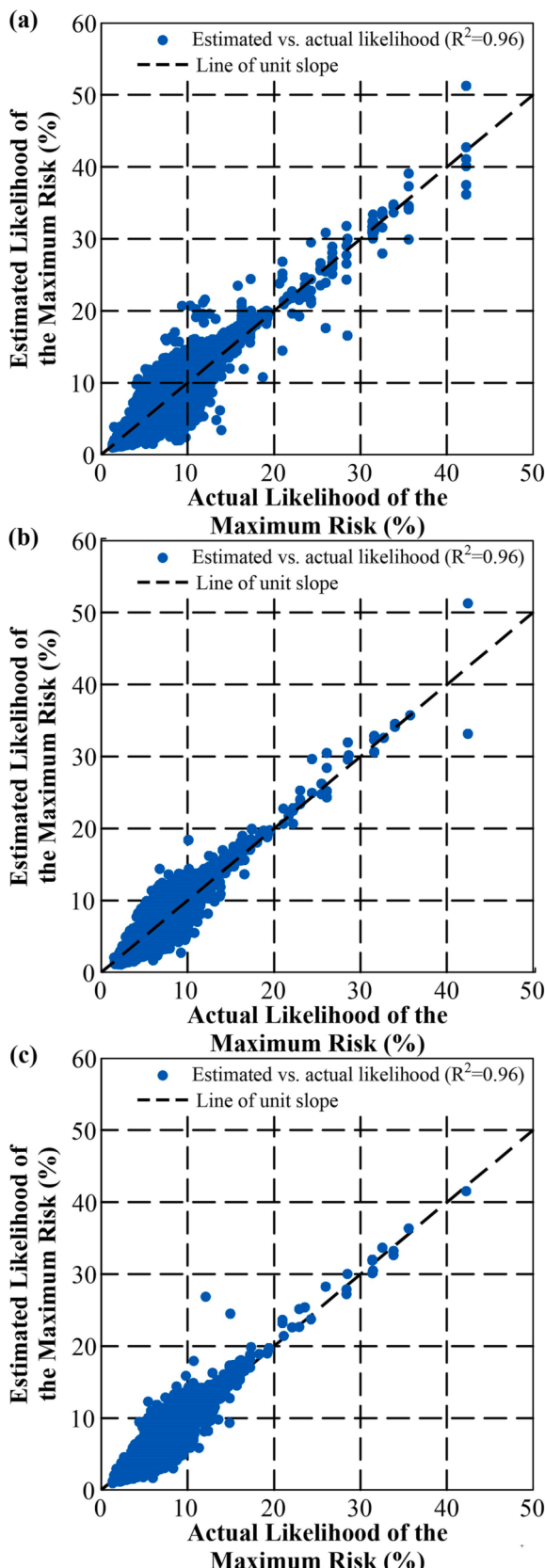


Fig. 10. HDNN-BMA model performance for the (a) training, (b) validation, and (c) testing subsets.

validation, and testing subsets. The high performance of the developed model for the testing subset, in particular, is an indication that overfitting was avoided, rendering the model generalizable to independent (i.e., unseen) datasets. In addition, the dispersion of errors (i.e., difference between estimated and actual values) around the 45-degree line is relatively small and symmetrically scattered for the three subsets, supporting that such errors are independent and identically distributed. For the maximum risk level estimation, the classification-based HDNN replicated the actual observations with total accuracies of 0.90, 0.85 and 0.80 for the training, validation, and testing, respectively. Additional performance metrics (i.e., recall, precision, and f-score) for each of the three subsets are summarized in Table 2. It should be noted that misclassification errors were larger for the very low and low risk classes compared to higher risk levels due to the unbalanced nature of actual risk levels (i.e., more than 74 % of the actual risk levels are medium or high).

4.2. Climate scenario-driven future risk predictions

RAPFLO was employed to predict the risk characteristics (maximum level and corresponding likelihood) for the City of Calgary between the years 2025 and 2100 under RCP 8.5 climate scenarios. As mentioned earlier, future climate indices used in this study are obtained from 24 global climate models. For demonstration, the following results and discussion focus on the RCP 8.5 climate scenario and the 50th percentile of the 24 global climate models indices only. Under such conditions and between 2025 and 2100, more than 50 % of the vulnerable area in the City of Calgary is expected to be in high flood risk, about 10–15 % will be in medium flood risk, whereas the remaining areas are anticipated to be in low or very low risk conditions (Fig. 11). It should be highlighted that areas under very high fluvial flood risk represent a significantly small fraction (<0.1 %) and are expected to be under such conditions for only a few years between 2025 and 2100. In addition, there is no consistent trend for the fluvial flood severity (i.e., when fluvial floods are expected to be mild or severe) under the considered climate scenario between the years 2025 and 2100. Fig. 11b shows the likelihood of each risk level averaged over the corresponding area within the city of Calgary from 2025 to 2100. The likelihood seems to be increasing for all risk levels towards the end of the period in 2100, albeit with an inconsistent trend. Such predictions highlight the alarming conditions that the City of Calgary will be exposed to in the near future, rendering the need for effective flood mitigation strategies. It should be noted that RAPFLO required only seconds/minutes to predict the annual flood risk

Table 2
Classification-based HDNN performance.

Risk level	Performance metric	Training	Validation	Testing
Very low	Precision	0.84	0.74	0.75
	Recall	0.81	0.72	0.75
	F-score	0.83	0.73	0.75
Low	Precision	0.82	0.76	0.75
	Recall	0.85	0.78	0.76
	F-score	0.84	0.77	0.75
Medium	Precision	0.86	0.79	0.79
	Recall	0.84	0.75	0.75
	F-score	0.85	0.77	0.77
High	Precision	0.91	0.85	0.85
	Recall	0.92	0.87	0.88
	F-score	0.91	0.86	0.86
Very high	Precision	0.92	0.81	0.83
	Recall	0.84	0.77	0.73
	F-score	0.88	0.79	0.78

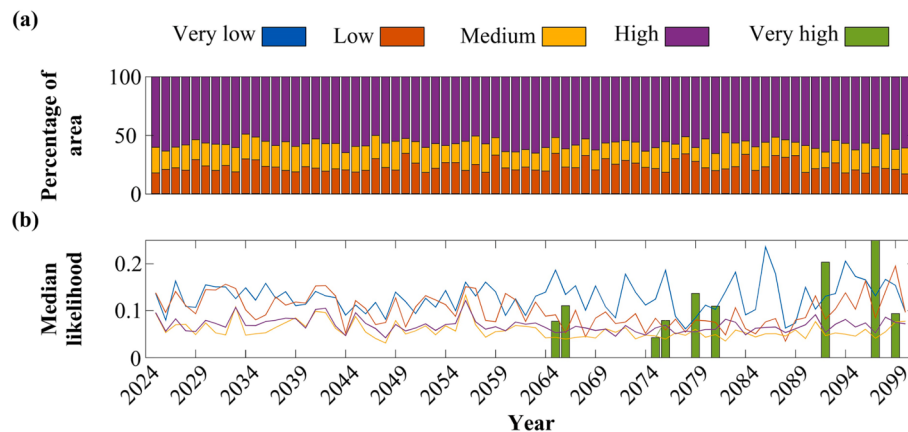


Fig. 11. RAPFLO predictions between 2050 and 2100 under RCP 8.5: (a) risk level and (b) likelihood.

characteristics over the City of Calgary study area compared to a matter of hours/days used by the corresponding HEC-RAS model to only estimate the annual inundation depth over the same area.

For further demonstration of the predictability of RAPFLO, the spatial distribution of the maximum expected fluvial flood risk level, likelihood, and corresponding induced damages across the City of Calgary in 2050 are shown in Fig. 12. About 50 % of vulnerable areas within the city is expected to be at high risk (Fig. 12a), which confirms the same observation from Fig. 11. In addition, areas nearby the Bow and Elbow rivers as well as their tributaries are observed to be under high flood risk, with severity decreases as the distance from the river increases. Fig. 12b shows the likelihood of the flood risk irrespective of level. The risk likelihood during 2050 is most probably less than 7%; however, some places near the Fish Creek and the downstream areas have a higher risk (between 13% and 45%). Fig. 12c presents the expected damage cost corresponding to the risk level and likelihood shown in Fig. 12a and Fig. 12b, respectively. Similar to the observations from Fig. 12b, the damage cost per square meters is significantly low in most of the flood-prone areas (less than \$60/m²) and increases in locations near the downtown and the Fish Creek areas (between \$325/m² to \$1,000/m²). Such estimations can guide the decisionmakers in the City of Calgary to effectively allocate the available resources such that the expected flood consequences are efficiently mitigated.

The results of the demonstration application support the utility of RAPFLO as an accurate, powerful, computationally efficient risk quantification tool that bypasses the complex, uncertain physics-based models, and tedious manipulations typically necessary for such purpose. RAPFLO can be applied for climate resilience planning through resembling the temporal fluvial flood risk level or the expected damage as the decline in the system robustness under such hazard. Proactive mitigation and adaptation plans as well as recovery resources and time can be accordingly prepared, estimated and applied prior to, during, and post the flood event to facilitate the rapid restoration of the system performance after hazard realization. For example, flood protection structures can be added, new policies for buildings' elevations may be applied, probabilistic and dynamic climatic resilience planning and management schemes should be adopted, emergency crews should be provided, inhabitants of at-risk areas can be evacuated and be flood-insured, and impacted buildings and infrastructures should be rehabilitated guided by key resilience metrics. RAPFLO can also be retrained considering the impacts of individual and/or coupled mitigations measures, and be subsequently applied to evaluate the new system's robustness (i.e., sensitivity to maximum risk or expected damage) under different climate change scenarios both deterministically (i.e., at specific climate indices' levels) and probabilistically (i.e., considering the different percentiles of climate indices). The deviation between the system robustness levels with and without the application of mitigation

measures can thus be used to quantify its efficiency, propelling optimal climate adaptation strategy. It should be also noted that the methodology applied for RAPFLO development assumes a minimal change in the demographic distribution and land use. However, drastic future developments can be considered through i) providing more insightful projected information based on synthetic development scenarios during the model training stage to accommodate such expected changes; or ii) employing vulnerability-related attributes as additional model inputs. Hence, such approaches imply that the system vulnerability can be represented through temporal maps that change based on the different development strategies. Following such training/development schemes, RAPFLO remains an easy-to-use, reliable, rapid, and accurate tool to evaluate the flood risk characteristics considering the climate change impacts together with those of the different urban development strategies and demographic variability scenarios within the area of interest. It should be highlighted that other assumptions adopted for RAPFLO development include those inherent within the data used for the HDNN training, testing, and validation. Examples include assumptions pertaining to flood depth estimation using the HEC-RAS model (e.g., model formulation, solver adopted, and calibration) as well as the assumptions related to homogenizing the vulnerability factors over the grid cells.

5. Conclusions

Extreme weather events are getting more intense, catastrophic, and frequent due to climate change. Fluvial floods, among other weather extremes, can propagate over large areas, resulting in significant human and monetary losses. With the ongoing intention of people to live in urban centers, fluvial flood risk quantification and prediction become more essential. The use of hydrologic and hydraulic models for hazard quantification is a well-established practice despite the inherited challenges such as the exorbitant computational cost and the complex integrated calibration. On the other hand, vulnerability assessment as part of the risk quantification process necessities collecting a massive amount of data that barely changes over shorter times as well as conducting tedious subjective/objective manipulations. The present study thus develops a data-driven tool for the accurate rapid prediction of flood risk, RAPFLO, that links the fluvial flood drivers (e.g., climate, topography, land cover) to the vulnerability drivers of the elements at-risk (e.g., population demography and gender distribution, infrastructure age and construction material) and directly relates both to the characteristics of the resulting risk (i.e., level, likelihood), bypassing the time-consuming risk quantification methodology described above. The computational core of RAPFLO is a hierachal deep neural network, HDNN, used individually for risk level estimation and integrated with the Bayesian model averaging technique for likelihood quantification. To demonstrate its utility, RAPFLO was first employed to assess historical fluvial

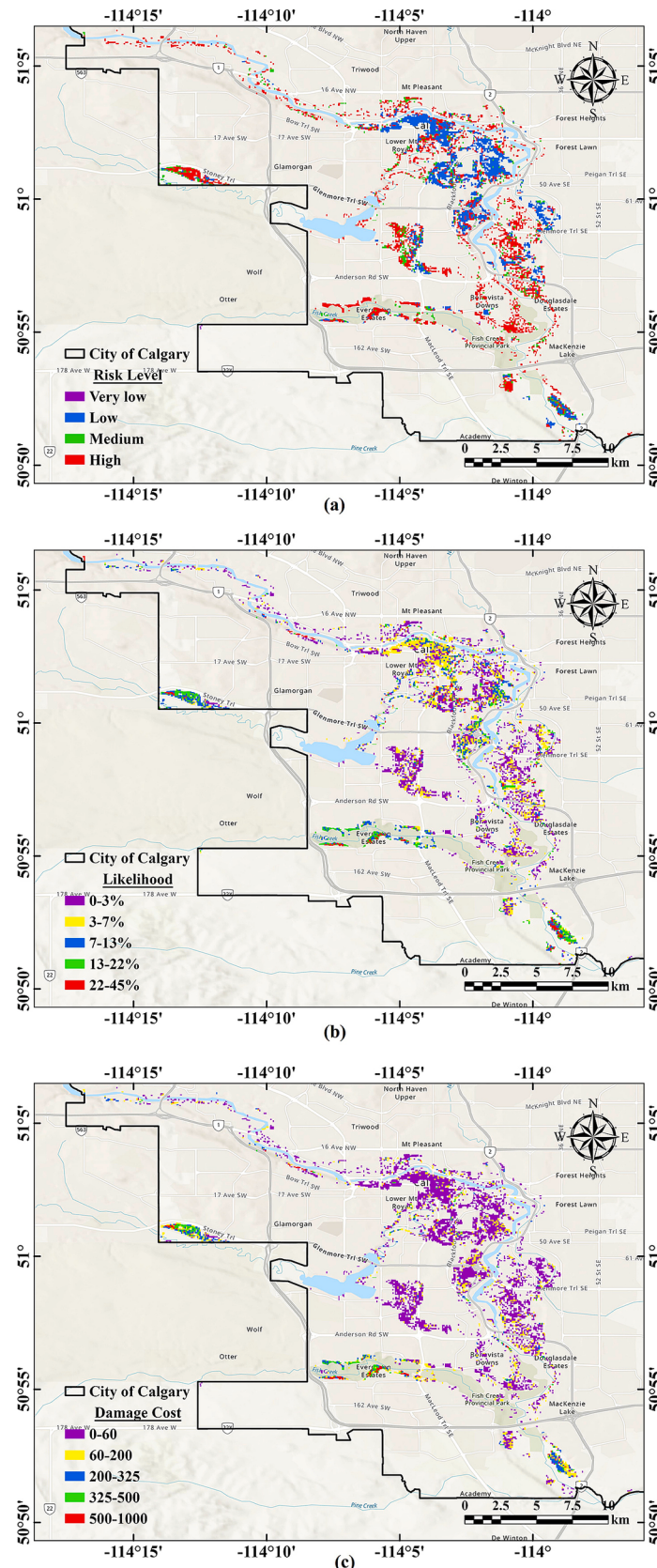


Fig. 12. Flood risk predictions in 2050 under RCP 8.5 scenario: (a) maximum risk level, (b) likelihood of the maximum risk, and (c) the corresponding damage cost per square meters evaluated based on 2014's money value.

flood risks in the city of Calgary, Canada, between 2010 and 2020, and subsequently for future risk predictions between 2025 and 2100 under the RCP 8.5 climate scenario. RAPFLO accurately estimated the fluvial flood risk maximum likelihood from 2010 to 2020 with an R^2 value of 0.96 during the training, validation, and testing stages. For risk level estimation, RAPFLO efficiently reproduced the actual values between 2010 and 2020 with a total accuracy of 80 %. For the prediction interval (between 2025 and 2100), the use of RAPFLO indicated that more than half of the fluvial flood-prone areas will be consistently susceptible to high risk levels and less than 0.1 % will be under very high risk levels during multiple years only. Further investigation of the risk predictions in 2050 shows that most of the vulnerable areas are exposed to a lower risk likelihood (<7%), with higher likelihoods, levels, and induced damage in areas near the main river systems and within the city's downtown. Such results support the utility of RAPFLO as a stand-alone tool that can be adopted by policy- and decisionmakers for the development of efficient preparedness plans to combat the devastating impacts of climate-induced fluvial floods. RAPFLO can also be employed to devise and evaluate different sustainable development strategies and climate resilience planning alternatives under future climate projections and what-if flood scenarios at the infrastructure, neighborhood, and city levels.

CRediT authorship contribution statement

Ahmed Yosri: Writing – review & editing, Writing – original draft, Visualization, Software, Methodology, Investigation, Formal analysis, Conceptualization. **Maysara Ghaith:** Writing – review & editing, Writing – original draft, Visualization, Validation, Software, Methodology, Investigation, Formal analysis, Conceptualization. **Wael El-Dakhakhni:** Writing – review & editing, Writing – original draft, Supervision, Project administration, Funding acquisition, Conceptualization.

Declaration of competing interest

The author declares the following financial interests/personal relationships which may be considered as potential competing interests: Wael El-Dakhakhni reports financial support provided by the Natural Sciences and Engineering Research Council of Canada (NSERC) through the Discovery Grant number [RGPIN-2021-03983]. Wael El-Dakhakhni has a related patent, Rapid Deep Learning-based Flood Losses/Risk Prediction Tool, methods of making and uses thereof, No. 63/533,240 pending to United States Provisional Application. The remaining authors declare that they have no known competing financial interests or personal relationships that could have appeared to influence the work reported in this paper.

Data availability

Data will be made available on request.

Acknowledgments

This research was supported by the Natural Sciences and Engineering Research Council of Canada (NSERC) through the Discovery Grant number [RGPIN-2021-03983].

References

- Ahmadi, A., Nasseri, M., Solomatine, D.P., 2019. Parametric uncertainty assessment of hydrological models: coupling UNEEC-P and a fuzzy general regression neural network. *Hydrol. Sci. J.* 64, 1080–1094. <https://doi.org/10.1080/02626667.2019.1610565>.
- Anaraki, M.V., Farzin, S., Mousavi, S.F., Karami, H., 2021. Uncertainty analysis of climate change impacts on flood frequency by using hybrid machine learning methods. *Water Resour. Manag.* 35, 199–223. <https://doi.org/10.1007/s11269-020-02719-w>.
- Aroca-Jiménez, E., Bodoque, J.M., García, J.A., Díez-Herrero, A., 2018. A quantitative methodology for the assessment of the regional economic vulnerability to flash floods. *J. Hydrol. (Amst)* 565, 386–399. <https://doi.org/10.1016/j.jhydrol.2018.08.029>.
- Aroca-Jiménez, E., Bodoque, J.M., García, J.A., Figueroa-García, J.E., 2022. Holistic characterization of flash flood vulnerability: Construction and validation of an integrated multidimensional vulnerability index. *J. Hydrol. (Amst)* 612. <https://doi.org/10.1016/j.jhydrol.2022.128083>.
- Balica, S.F., Douben, N., Wright, N.G., 2009. Flood vulnerability indices at varying spatial scales. *Water Sci. Technol.* 60, 2571–2580. <https://doi.org/10.2166/wst.2009.183>.
- Boomsma, W., Ferkinghoff-Borg, J., Lindorff-Larsen, K., 2014. Combining experiments and simulations using the maximum entropy principle. *PLoS Comput. Biol.* 10. <https://doi.org/10.1371/journal.pcbi.1003406>.
- Buchanan, T., Ackland, J., Lloyd, S., van der Linden, S., de-Wit, L., 2022. Clear consensus among international public for government action at COP26: Patriotic and public health frames produce marginal gains in support. *Clim. Change.* <https://doi.org/10.1007/s10584-021-03262-2>.
- Calgary, 2021. <http://www.calgary.ca/> [WWW Document].
- Cea, L., Costabile, P., 2022. Flood risk in urban areas: modelling, management and adaptation to climate change: A review. *Hydrology*.
- Chang, L.C., Wang, W.H., Chang, F.J., 2021. Explore training self-organizing map methods for clustering high-dimensional flood inundation maps. *J. Hydrol. (Amst)* 595. <https://doi.org/10.1016/j.jhydrol.2020.125655>.
- Chang, L.C., Liou, J.Y., Chang, F.J., 2022. Spatial-temporal flood inundation nowcasts by fusing machine learning methods and principal component analysis. *J. Hydrol. (Amst)* 612. <https://doi.org/10.1016/j.jhydrol.2022.128086>.
- Chen, J., Huang, G., Chen, W., 2021. Towards better flood risk management: Assessing flood risk and investigating the potential mechanism based on machine learning models. *J. Environ. Manage.* 293. <https://doi.org/10.1016/j.jenvman.2021.112810>.
- Cheng, Y., Sinha, A., Ghosh, V., Sengupta, T., Luo, H., 2021. Carbon tax and energy innovation at crossroads of carbon neutrality: Designing a sustainable decarbonization policy. *J. Environ. Manage.* 294. <https://doi.org/10.1016/j.jenvman.2021.112957>.
- Cho, S.Y., Chang, H., 2017. Recent research approaches to urban flood vulnerability, 2006–2016. *Nat. Hazards.* <https://doi.org/10.1007/s11069-017-2869-4>.
- da Silva, L.B.L., Alencar, M.H., de Almeida, A.T., 2020. Multidimensional flood risk management under climate changes: Bibliometric analysis, trends and strategic guidelines for decision-making in urban dynamics. *Int. J. Disaster Risk Reduct.* <https://doi.org/10.1016/j.ijdr.2020.101865>.
- da Silva, L.B.L., Alencar, M.H., de Almeida, A.T., 2022. A novel spatiotemporal multi-attribute method for assessing flood risks in urban spaces under climate change and demographic scenarios. *Sustain. Cities Soc.* 76. <https://doi.org/10.1016/j.scs.2021.103501>.
- Dewan, A.M., 2013. In: Floods in a Megacity: Geospatial Techniques in Assessing Hazards, Risk and Vulnerability. Springer, Dordrecht Heidelberg. <https://doi.org/10.1007/978-94-007-5875-9>.
- Duan, Q., Ajami, N.K., Gao, X., Sorooshian, S., 2007. Multi-model ensemble hydrologic prediction using Bayesian model averaging. *Adv. Water Resour.* 30, 1371–1386. <https://doi.org/10.1016/j.advwatres.2006.11.014>.
- Eini, M., Kaboli, H.S., Rashidian, M., Hedayat, H., 2020. Hazard and vulnerability in urban flood risk mapping: Machine learning techniques and considering the role of urban districts. *Int. J. Disaster Risk Reduct.* 50. <https://doi.org/10.1016/j.ijdr.2020.101687>.
- Ekmekcioglu, Ö., Koc, K., Özger, M., 2022. Towards flood risk mapping based on multi-tiered decision making in a densely urbanized metropolitan city of Istanbul. *Sustain. Cities Soc.* 80, 103759. <https://doi.org/10.1016/j.scs.2022.103759>.
- Emdad Haque, C., Mahmud, K.H., Walker, D., Zaman, J.R., 2022. Geophysical and societal dimensions of floods in Manitoba, Canada: A social vulnerability assessment of the rural municipality of St. Andrews. *Geosciences (Switzerland)* 12. <https://doi.org/10.3390/geosciences12020056>.
- Fekete, H., Kuramochi, T., Roelfsema, M., den Elzen, M., Forsell, N., Höhne, N., Luna, L., Hans, F., Sterl, S., Olivier, J., van Soest, H., Frank, S., Gusti, M., 2021. A review of successful climate change mitigation policies in major emitting economies and the potential of global replication. *Renew. Sustain. Energy Rev.* 137. <https://doi.org/10.1016/j.rser.2020.110602>.
- Feng, Q., Liu, J., Gong, J., 2015. Urban flood mapping based on unmanned aerial vehicle remote sensing and random forest classifier-A case of yuyao, China. *Water (Switzerland)* 7, 1437–1455. <https://doi.org/10.3390/w7041437>.
- Ficklin, D.L., Barnhart, B.L., 2014. SWAT hydrologic model parameter uncertainty and its implications for hydroclimatic projections in snowmelt-dependent watersheds. *J. Hydrol. (Amst)* 519 (Part B), 2081–2090. <https://doi.org/10.1016/j.jhydrol.2014.09.082>.
- Fuchs, S., Keiler, M., Ortlepp, R., Schinke, R., Papathoma-Köhle, M., 2019. Recent advances in vulnerability assessment for the built environment exposed to torrential hazards: Challenges and the way forward. *J. Hydrol. (Amst)*. <https://doi.org/10.1016/j.jhydrol.2019.05.067>.
- Gaur, A., Gaur, A., Simonovic, S.P., 2018b. Modelling of future flood risk across Canada due to climate change, in: *WIT Transactions on Engineering Sciences*. WITPress, pp. 149–159. <https://doi.org/10.2495/RISK180131>.
- Gaur, A., Gaur, A., Simonovic, S.P., 2018a. Future changes in flood hazards across Canada under a changing climate. *Water* 10. <https://doi.org/10.3390/w10101441>.
- Ghaith, M., Yosri, A., El-dakhakhni, W., 2022b. Digital Twin: A City-Scale Flood Imitation Framework, in: *The Canadian Society of Civil Engineering Annual*

- Conference 2021. CSCE, Montreal, Canada, pp. 577–588. https://doi.org/10.1007/978-981-19-1065-4_48.
- Ghaith, M., Yosri, A., El-Dakhkhni, W., 2022a. Synchronization-enhanced deep learning early flood risk predictions: The core of data-driven city digital twins for climate resilience planning. *Water (Basel)* 14, 3619. <https://doi.org/10.3390/w14223619>.
- Government of Canada, 2022. <https://www.canada.ca/> [WWW Document].
- Haykin, S., 1999. *Neural Networks: A Comprehensive Foundation*, Second Ed. Prentice-Hall PTR, Upper Saddle River, New Jersey.
- He, R., Chen, Y., Liu, Y., Pan, Z., Huang, Q., 2023. Two strategies for avoiding overfitting long-term forecasting models: Downsampling predictor fields and shrinking coefficients. *J. Hydrol. Eng.* 28 <https://doi.org/10.1061/j.hydro.2023.126239>.
- Hou, J., Zhou, N., Chen, G., Huang, M., Bai, G., 2021. Rapid forecasting of urban flood inundation using multiple machine learning models. *Nat. Hazards* 108, 2335–2356. <https://doi.org/10.1007/s11069-021-04782-x>.
- Huang, M., Liang, X., 2006. On the assessment of the impact of reducing parameters and identification of parameter uncertainties for a hydrologic model with applications to ungauged basins. *J. Hydrol.* 37–61. <https://doi.org/10.1016/j.jhydrol.2005.07.010>.
- Jang, J.H., Hsieh, C.Y., Li, T.W., 2022. Flood mapping based on the combination of support vector regression and Heun's scheme. *J. Hydrol.* 613, 128477. <https://doi.org/10.1016/j.jhydrol.2022.128477>.
- Jenifer, M.A., Jha, M.K., 2017. Comparison of analytic hierarchy process, catastrophe and entropy techniques for evaluating groundwater prospect of hard-rock aquifer systems. *J. Hydrol. (Amst)* 548, 605–624. <https://doi.org/10.1016/j.jhydrol.2017.03.023>.
- Jhong, Y.D., Lin, H.P., Chen, C.S., Jhong, B.C., 2022. Real-time neural-network-based ensemble typhoon flood forecasting model with self-organizing map cluster analysis: A case study on the Wu River Basin in Taiwan. *Water Resour. Manag.* 36, 3221–3245. <https://doi.org/10.1007/s11269-022-03197-y>.
- Johansson, E.M., Dowla, F.U., Goodman, D.M., 1992. Backpropagation learning for multilayer feed-forward neural networks using the conjugate gradient method. *Int. J. Neural Syst.* 2, 291–301.
- Kabir, S., Patidar, S., Xia, X., Liang, Q., Neal, J., Pender, G., 2020. A deep convolutional neural network model for rapid prediction of fluvial flood inundation. *J. Hydrol. (Amst)* 590, 125481. <https://doi.org/10.1016/j.jhydrol.2020.125481>.
- Keum, J., Kornelsen, K.C., Leach, J.M., Coulibaly, P., 2017. Entropy applications to water monitoring network design: A review. *Entropy*. <https://doi.org/10.3390/e19110613>.
- Keum, J., Coulibaly, P., Razavi, T., Tapsoba, D., Gobena, A., Weber, F., Pietroniro, A., 2018. Application of SNODAS and hydrologic models to enhance entropy-based snow monitoring network design. *J. Hydrol. (Amst)* 561, 688–701. <https://doi.org/10.1016/j.jhydrol.2018.04.037>.
- Khan, U.T., He, J., Valeo, C., 2018. River flood prediction using fuzzy neural Networks: An investigation on automated network architecture. *Water Sci. Technol.* 2017, 238–247. <https://doi.org/10.2166/wst.2018.107>.
- Komolafe, A.A., Herath, S., Avtar, R., 2018. Methodology to assess potential flood damages in urban areas under the influence of climate change. *Nat. Hazards Rev.* 19 [https://doi.org/10.1061/\(ASCE\)NH.1527-6996.0000278](https://doi.org/10.1061/(ASCE)NH.1527-6996.0000278).
- Kumar, V., Azamathulla, H.M., Sharma, K.V., Mehta, D.J., Maharaj, K.T., 2023. The state of the art in deep learning applications, challenges, and future prospects: A comprehensive review of flood forecasting and management. *Sustainability (Switzerland)*. <https://doi.org/10.3390/su151310543>.
- Lai, C., Chen, X., Chen, X., Wang, Z., Wu, X., Zhao, S., 2015. A fuzzy comprehensive evaluation model for flood risk based on the combination weight of game theory. *Nat. Hazards* 77, 1243–1259. <https://doi.org/10.1007/s11069-015-1645-6>.
- Li, Z., Chen, M., Gao, S., Luo, X., Gourley, J.J., Kirstetter, P., Yang, T., Kolar, R., McGovern, A., Wen, Y., Rao, B., Yami, T., Hong, Y., 2021. CREST-iMAP v1.0: A fully coupled hydrologic-hydraulic modeling framework dedicated to flood inundation mapping and prediction. *Environ. Model. Softw.* 141 <https://doi.org/10.1016/j.envsoft.2021.105051>.
- Li, S., Wang, Z., Lai, C., Lin, G., 2020. Quantitative assessment of the relative impacts of climate change and human activity on flood susceptibility based on a cloud model. *J. Hydrol. (Amst)* 588. <https://doi.org/10.1016/j.jhydrol.2020.125051>.
- Li, G., Zhang, X., Cannon, A.J., Murdock, T., Sobie, S., Zwiers, F., Anderson, K., Qian, B., 2018. Indices of Canada's future climate for general and agricultural adaptation applications. *Clim. Change* 148, 249–263. <https://doi.org/10.1007/s10584-018-2199-x>.
- Lianxiao, Morimoto, T., 2019. Spatial analysis of social vulnerability to floods based on the MOVE framework and information entropy method: Case study of Katsushika Ward, Tokyo. *Sustainability (Switzerland)* 11. <https://doi.org/10.3390/su11020529>.
- Liao, Y., Wang, Z., Chen, X., Lai, C., 2023. Fast simulation and prediction of urban pluvial floods using a deep convolutional neural network model. *J. Hydrol. (Amst)* 624. <https://doi.org/10.1016/j.jhydrol.2023.129945>.
- Marco, Z., Elena, A., Anna, S., Silvia, T., Andrea, C., 2022. Spatio-temporal cross-validation to predict pluvial flood events in the Metropolitan City of Venice. *J. Hydrol. (Amst)* 612. <https://doi.org/10.1016/j.jhydrol.2022.128150>.
- McLennan, M., 2021. *The Global Risks Report 2021*, 16th Ed.
- McLennan, M., 2022. *The Global Risks Report 2022*, 17th Ed.
- Mehravar, S., Razavi-Termeh, S.V., Moghimi, A., Ranjbar, B., Foroughnia, F., Amani, M., 2023. Flood susceptibility mapping using multi-temporal SAR imagery and novel integration of nature-inspired algorithms into support vector regression. *J. Hydrol.* 617, 129100. <https://doi.org/10.1016/j.jhydrol.2023.129100>.
- Membele, G.M., Naidu, M., Mutanga, O., 2022. Examining flood vulnerability mapping approaches in developing countries: A scoping review. *Int. J. Disaster Risk Reduct.* <https://doi.org/10.1016/j.ijdrr.2021.102766>.
- Misra, B., Prigogine, I., Courbage, M., 1979. Lyapounov variable: Entropy and measurement in quantum mechanics. *Physics*.
- Mohanty, M.P., Simonovic, S.P., 2021. Fidelity of reanalysis datasets in floodplain mapping: Investigating performance at inundation level over large regions. *J. Hydrol. (Amst)* 597. <https://doi.org/10.1016/j.jhydrol.2020.125757>.
- Moreira, L.L., de Brito, M.M., Kobiyama, M., 2021. Review article: A systematic review and future prospects of flood vulnerability indices. *Nat. Hazards Earth Syst. Sci.* <https://doi.org/10.5194/nhess-21-1513-2021>.
- Nofal, O.M., van de Lindt, J.W., 2020. Understanding flood risk in the context of community resilience modeling for the built environment: research needs and trends. *Sustain. Resilient Infrastruct.* <https://doi.org/10.1080/23789689.2020.1722546>.
- Norallahi, M., Seyed Kaboli, H., 2021. Urban flood hazard mapping using machine learning models: GARP, RF, MaxEnt and NB. *Nat. Hazards* 106, 119–137. <https://doi.org/10.1007/s11069-020-04453-3>.
- Oubennaceur, K., Chokmani, K., Gauthier, Y., Ratte-Fortin, C., Homayouni, S., Toussaint, J.P., 2021. Flood risk assessment under climate change: The petite nation river watershed. *Climate* 9. <https://doi.org/10.3390/cl9080125>.
- Pal, N.R., Pal, S.K., 1991. Entropy: A new definition and its applications. *Trans. Syst. Man Cybernet.* 21.
- Papathoma-Köhle, M., Schlägl, M., Dosser, L., Roesch, F., Borga, M., Erlicher, M., Keiler, M., Fuchs, S., 2022. Physical vulnerability to dynamic flooding: Vulnerability curves and vulnerability indices. *J. Hydrol. (Amst)* 607. <https://doi.org/10.1016/j.jhydrol.2022.127501>.
- Pasquier, U., He, Y., Hooton, S., Goulden, M., Hiscock, K.M., 2019. An integrated 1D–2D hydraulic modelling approach to assess the sensitivity of a coastal region to compound flooding hazard under climate change. *Nat. Hazards* 98, 915–937. <https://doi.org/10.1007/s11069-018-3462-1>.
- Purvis, B., Mao, Y., Robinson, D., 2019. Entropy and its application to urban systems. *Entropy* 21. <https://doi.org/10.3390/e21010056>.
- Raftery, A.E., Gneiting, T., Balabdaoui, F., Polakowski, M., 2005. Using Bayesian Model Averaging to Calibrate Forecast Ensembles.
- Rasheed, Z., Aravamudan, A., Gorji Sefidmazgi, A., Anagnostopoulos, G.C., Nikolopoulos, E.I., 2022. Advancing flood warning procedures in ungauged basins with machine learning. *J. Hydrol. (Amst)* 609. <https://doi.org/10.1016/j.jhydrol.2022.127736>.
- Scawthorn, C., Asce, F., Flores, P., Blais, N., Seligson, H., Tate, E., Chang, S., Mifflin, E., Thomas, W., Murphy, J., Jones, C., Lawrence, M., 2006. HAZUS-MH flood loss estimation methodology. II. Damage and loss assessment. *Nat. Hazards. Rev.* 7, 72–81. <https://doi.org/10.1061/ASCE1527-698820067:272>.
- Smith, D.I., 1994. Flood damage estimation-A review of urban stage-damage curves and loss functions. *Water SA* 20, 231–238. https://doi.org/10.10520/AJA03784738_1124.
- Srivastava, N., Hinton, G., Krizhevsky, A., Salakhutdinov, R., 2014. Dropout: A simple way to prevent neural networks from overfitting. *J. Mach. Learn. Res.*
- Ursulak, J., Coulibaly, P., 2021. Integration of hydrological models with entropy and multi-objective optimization based methods for designing specific needs streamflow monitoring networks. *J. Hydrol. (Amst)* 593. <https://doi.org/10.1016/j.jhydrol.2020.125876>.
- Verma, S., Verma, M.K., Prasad, A.D., Mehta, D., Azamathulla, H.M., Muttill, N., Rathnayake, U., 2023. Simulating the hydrological processes under multiple land use/land cover and climate change scenarios in the Mahanadi reservoir complex, Chhattisgarh, India. *Water (Switzerland)* 15. <https://doi.org/10.3390/w15173068>.
- Wan Mohar, W.H.M., Abdullah, J., Abdul Maulud, K.N., Muhammad, N.S., 2020. Urban flash flood index based on historical rainfall events. *Sustain. Cities Soc.* 56 <https://doi.org/10.1016/j.scs.2020.102088>.
- Wu, J., Chen, X., Lu, J., 2022. Assessment of long and short-term flood risk using the multi-criteria analysis model with the AHP-Entropy method in Po Yang Lake basin. *Int. J. Disaster Risk Reduct.* 75. <https://doi.org/10.1016/j.ijdrr.2022.102968>.
- Yan, X., Mohammadian, A., Khelifa, A., 2021. Modeling spatial distribution of flow depth in fluvial systems using a hybrid two-dimensional hydraulic-multigene genetic programming approach. *J. Hydrol. (Amst)* 600. <https://doi.org/10.1016/j.jhydrol.2021.126517>.
- Yan, X., Mohammadian, A., Ao, R., Liu, J., Yang, N., 2023. Two-dimensional convolutional neural network outperforms other machine learning architectures for water depth surrogate modeling. *J. Hydrol. (Amst)* 616. <https://doi.org/10.1016/j.jhydrol.2022.128812>.
- Yelon, A., Movaghfar, B., Crandall, R.S., 2006. Multi-excitation entropy: Its role in thermodynamics and kinetics. *Rep. Prog. Phys.* 69, 1145–1194. <https://doi.org/10.1088/0034-4885/69/4/R04>.
- Youssef, A.M., Pradhan, B., Sefry, S.A., 2016. Flash flood susceptibility assessment in Jeddah city (Kingdom of Saudi Arabia) using bivariate and multivariate statistical models. *Environ. Earth Sci.* 75, 1–16. <https://doi.org/10.1007/s12665-015-4830-8>.
- Yu, J., Castellani, K., Forysinski, K., Gustafson, P., Lu, J., Peterson, E., Tran, M., Yao, A., Zhao, J., Brauer, M., 2021a. Geospatial indicators of exposure, sensitivity, and adaptive capacity to assess neighbourhood variation in vulnerability to climate change-related health hazards. *Environ. Health* 20. <https://doi.org/10.1186/s12940-021-00708-z>.
- Yu, J., Kim, J.E., Lee, J.H., Kim, T.W., 2021b. Development of a PCA-based vulnerability and copula-based hazard analysis for assessing regional drought risk. *KSCE J. Civ. Eng.* 25, 1901–1908. <https://doi.org/10.1007/s12205-021-0922-z>.

- Zandalinas, S.I., Fritschi, F.B., Mittler, R., 2021. Global warming, climate change, and environmental pollution: Recipe for a multifactorial stress combination disaster. *Trends Plant Sci.* <https://doi.org/10.1016/j.tplants.2021.02.011>.
- Zanotti, C., Rotiroti, M., Sterlacchini, S., Cappellini, G., Fumagalli, L., Stefania, G.A., Nannucci, M.S., Leoni, B., Bonomi, T., 2019. Choosing between linear and nonlinear models and avoiding overfitting for short and long term groundwater level forecasting in a linear system. *J. Hydrol. (Amst)* 578. <https://doi.org/10.1016/j.jhydrol.2019.124015>.
- Zhang, L., Qin, H., Mao, J., Cao, X., Fu, G., 2023. High temporal resolution urban flood prediction using attention-based LSTM models. *J. Hydrol. (Amst)* 620. <https://doi.org/10.1016/j.jhydrol.2023.129499>.
- Zhang, X., Wang, C., Li, E., Xu, C., 2014. Assessment model of ecoenvironmental vulnerability based on improved entropy weight method. *Sci. World J.* 2014 <https://doi.org/10.1155/2014/797814>.
- Zhou, Y., Wu, W., Nathan, R., Wang, Q.J., 2021. A rapid flood inundation modelling framework using deep learning with spatial reduction and reconstruction. *Environ. Model. Softw.* 143 <https://doi.org/10.1016/j.envsoft.2021.105112>.
- Zhu, Y., Tian, D., Yan, F., 2020. Effectiveness of entropy weight method in decision-making. *Math. Probl. Eng.* 2020 <https://doi.org/10.1155/2020/3564835>.
- Ziarh, G.F., Asaduzzaman, M., Dewan, A., Nashwan, M.S., Shahid, S., 2021. Integration of catastrophe and entropy theories for flood risk mapping in peninsular Malaysia. *J. Flood Risk Manag.* 14 <https://doi.org/10.1111/jfr3.12686>.
- Zou, Y., Wang, J., Lei, P., Li, Y., 2023. A novel multi-step ahead forecasting model for flood based on time residual LSTM. *J. Hydrol. (Amst)* 620. <https://doi.org/10.1016/j.jhydrol.2023.129521>.